Soft Matter

ARTICLE TYPE

Cite this: DOI: 00.0000/xxxxxxxxxx

Modeling the assembly of oppositely charged *lock*- and *key*-colloids

Björn Stenqvist,*[a] Martin Trulsson,[b] and Jérôme J. Crassous[ac‡]

Received Date
Accepted Date

DOI: 00.0000/xxxxxxxxxx

Interaction-energy between *lock*- and *key*-particles

In this section we present the electrostatic Yukawa-potential $V_L(z)$, from a *lock*-particle on the line parallel to $\mathbf{c} = \mathbf{C} - \mathbf{L}$ going through $\mathbf{L}$, see Fig. S1. The resulting Eq. S5 is based on calculations where the charge q_L of the *lock*-particle is uniformly distributed on its surface-area A, see Eq S1. In Eq. S5 κ^{-1} is the Debye-length, $\angle\mathbf{RLC}$ and $\angle\mathbf{RCL}$ are described in Eqs. S2-S3, ε_0 and ε_r are respectively the permittivitiy of vacuum and the relative permittivity of the dispersing medium. We define $\mathbf{R}$ as any point on the circle where the spheres $(\mathbf{L}, R_L)$ and $(\mathbf{C}, R_C)$ intersects, *i.e.* the rim of the cavity. Here a sphere is defined by its center point and radius. In Eq. S4, z is described as a function of the surface-to-surface distance d. An approximate expression for the interaction between an arc and a sphere has been derived elsewhere [1] yet in the following we have derived an exact expression for the same problem.

$$A = \frac{\pi}{c}\left(R_L^3 + (R_C + 2c)R_L^2 - (R_C^2 - c^2)R_L - (R_C - c)^2 R_C\right) \tag{S1}$$

$$\cos(\angle\mathbf{RLC}) = \frac{R_L^2 + c^2 - R_C^2}{2R_L c} \tag{S2}$$

$$\cos(\angle\mathbf{RCL}) = \frac{R_C^2 + c^2 - R_L^2}{2R_C c} \tag{S3}$$

[a] *Division of Physical Chemistry, Lund University, POB 124, SE-22100 Lund, Sweden.*
[b] *Division of Theoretical Chemistry, Lund University, POB 124, SE-22100 Lund, Sweden*
[c] *Institute of Physical Chemistry, RWTH Aachen University, Landoltweg 2, 52074, Aachen, Germany*
* *E-mail: bjorn.stenqvist@teokem.lu.se*
‡ *E-mail: crassous@pc.rwth-aachen.de*

† Electronic Supplementary Information (ESI) available: [details of any supplementary information available should be included here]. See DOI: 10.1039/b000000x/

$$z = \begin{cases} d + c - R_C & \forall\ z > c - R_C \\ -d - R_L & \forall\ z \leq -R_L \end{cases} \tag{S4}$$

There are two special cases for which the denominators in Eq. S5 becomes zero: $z = 0$ or $z = c$. The first term using $z \to 0$ in Eq. S5 is described in Eq. S6 whereas the second term using $z \to c$ is described in Eq. S7.

$$\begin{aligned} \frac{V_L(z)}{\left(\frac{q_L}{4\pi\varepsilon_0\varepsilon_r}\right)} = {} & \frac{2R_L\pi}{A\kappa z}\left[\exp\left(-\kappa\sqrt{R_L^2 - 2\cos(\angle\mathbf{RLC})R_L z + z^2}\right) - \exp(-\kappa|R_L + z|)\right] + \\ & + \frac{2R_C\pi}{A\kappa(z-c)}\left[\exp\left(-\kappa\sqrt{R_C^2 + 2\cos(\angle\mathbf{RCL})R_C(z-c) + (z-c)^2}\right) - \exp(-\kappa|R_C + z - c|)\right] \end{aligned} \tag{S5}$$

$$\lim_{z\to 0}\frac{2R_L\pi}{A\kappa z}\left[\exp\left(-\kappa\sqrt{R_L^2 - 2\cos(\angle\mathbf{RLC})R_L z + z^2}\right) - \exp(-\kappa|R_L + z|)\right] = \frac{2R_L\pi}{A}(\cos(\angle\mathbf{RLC}) + 1)e^{-\kappa R_L} \tag{S6}$$

$$\lim_{z\to c}\frac{2R_C\pi}{A\kappa(z-c)}\left[\exp\left(-\kappa\sqrt{R_C^2 + 2\cos(\angle\mathbf{RCL})R_C(z-c) + (z-c)^2}\right) - \exp(-\kappa|R_C + z - c|)\right] = -\frac{2R_C\pi}{A}(\cos(\angle\mathbf{RCL}) - 1)e^{-\kappa R_C} \tag{S7}$$

In the limit $\kappa \to 0$ we use the asymptotic limit

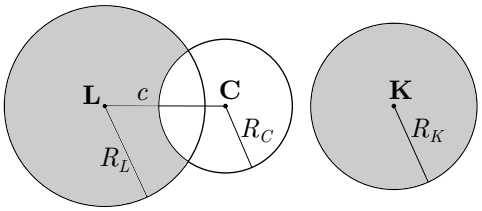

Fig. S1 Schematic illustration of a *lock*-particle and a *key*-particle where **K** is on the line parallel to $\mathbf{C}-\mathbf{L}$ going through **L**.

$$\lim_{x\to 0}\left(\frac{e^{Ax}-e^{Bx}}{x}\right)=A-B \tag{S8}$$

to get a valid expression for the potential.

The interaction energy between a *lock*- and a *key*-particle is retrieved by using Eq. S5 and the effective charge of the *key*-particle[2–4], $q_K^*=\frac{\sinh(\kappa R_K)}{\kappa R_K}q_K$, such that in the limit $\kappa R_K\to 0$, $q_K^*=q_K$. Here q_K is the charge of the *key*-particle. The resulting expression for the interaction-energy is $U_{LK}(z)=V_L(z)q_K^*$. In Fig. S2 we present the interaction energy between a *lock*- and a *key*-particle as a function of the normalized distance d/R_L, where U_{LK} and $U_{\overline{LK}}$ represent the two different cases in Eq. S4 and ΔU is the difference between the two.

Angular-dependent potential

The angular-dependent potential in the different regions is a linear combination of the exact expressions derived in the former section, where the *key*-particle is perfectly in front ($V_L(z_{LK}(\mathbf{r},\mathbf{c}))$) and behind ($V_L(z_{\overline{LK}}(\mathbf{r},\mathbf{c}))$) the *lock*-particle. Here

$$z_{LK}(\mathbf{r},\mathbf{c})=d(\mathbf{r},\mathbf{c})+c-R_C \tag{S9}$$

and

$$z_{\overline{LK}}(\mathbf{r},\mathbf{c})=-d(\mathbf{r},\mathbf{c})-R_L, \tag{S10}$$

where the closeted distance to contact

$$d(\mathbf{r},\mathbf{c})=\begin{cases}R_C-|\mathbf{r}-\mathbf{c}|-R_K & \text{Region I \& II}\\ |\mathbf{r}|-c+R_C-R_K & \text{Region III}\\ |\mathbf{r}|-R_L-R_K & \text{Region IV.}\end{cases} \tag{S11}$$

The potential is described by

$$V_L(\mathbf{r},\mathbf{c})=\lambda(\mathbf{r},\mathbf{c})V_L(z_{LK}(\mathbf{r},\mathbf{c}))+(1-\lambda(\mathbf{r},\mathbf{c}))V_L(z_{\overline{LK}}(\mathbf{r},\mathbf{c})), \tag{S12}$$

where $\lambda(\mathbf{r},\mathbf{c})$ is defined as follows. In Region I and Region III

$$\lambda_{\mathrm{I}}(\mathbf{r},\mathbf{c})=\lambda_{\mathrm{III}}(\mathbf{r},\mathbf{c})=\frac{\cos(\angle\mathbf{RCL})-\cos(\angle\mathbf{LCK})}{\cos(\angle\mathbf{RCL})-1}, \tag{S13}$$

in Region II

$$\lambda_{\mathrm{II}}(\mathbf{r},\mathbf{c})=\frac{\cos(\angle\mathbf{RLC})-\cos(\angle\mathbf{KLC})}{\cos(\angle\mathbf{RLC})-1}, \tag{S14}$$

and finally in Region IV

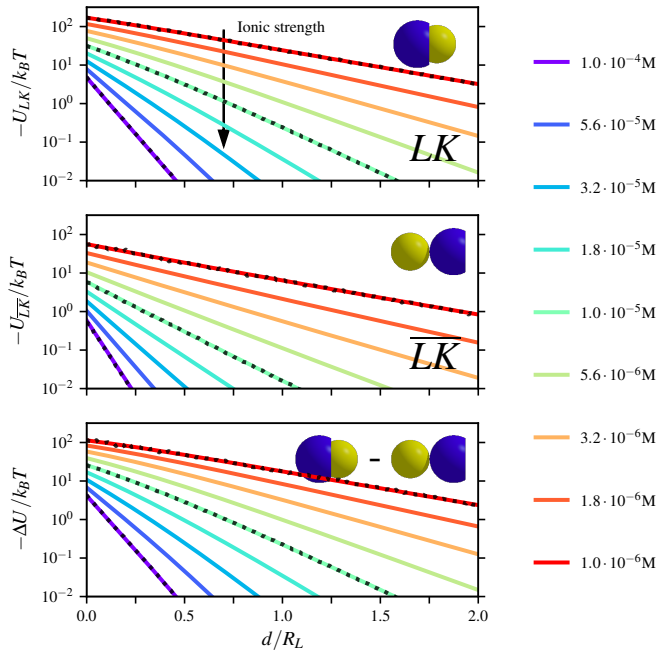

Fig. S2 Interaction-energy between a *lock*-particle and a *key*-particle as a function of the normalized distance to contact. The radius of the *key*-particle was $R_K=0.8R_L$, $R_L=R_C=c=500$ nm, and $|\sigma|=3.183\cdot10^{-4}$ e/nm^2. Energy calculations for the specific LK-configuration are shown in the top panel, for the unspecific $\overline{LK}$-configuration in the middle panel, and the difference between the two energies is displayed in the bottom panel. The gray dotted lines refer to explicit charge calculation using a *lock*-particle decorated with 10000 point-charges, and an effective charge of the *key*-particle for the ionic strengths 10^{-4} M, 10^{-5} M and 10^{-6} M.

$$\lambda_{\mathrm{IV}}(\mathbf{r},\mathbf{c})=0. \tag{S15}$$

There is one exception to the previous formulas, more precisely Eq. S11, and that is in $z_{\overline{LK}}(\mathbf{r},\mathbf{c})$ in Region III where $d=\sqrt{R_L^2+r^2-2R_Lr\cos(\angle\mathbf{RLC}-\angle\mathbf{KLC})}$, that is the closest distance to the rim of the *lock*-particle.

The model was compared to the potential obtained by randomly distributing 10000 point charges at the surface of the *lock*-particle. The results for different ionic strengths are summarized in Figs. S3-S5. The upper parts show a *lock*-particle where the surface is decorated with 10000 randomly positioned point-charges (left) and the approximate model (right). The lower parts show the potential from the respective models (left and middle) and the difference between the two (right).

Notes on the angular-dependent potential and the regions

- In Region I/II/III, given that $\{\angle\mathbf{LCK},\angle\mathbf{KLC},\angle\mathbf{LCK}\}=\{0,0,\pi\}$ (*i.e.* perfectly in front of the cavity of the *lock*-particle), the expression reduces to $V_L(\mathbf{r},\mathbf{c})=V_L(z_{LK}(\mathbf{r},\mathbf{c}))$ and is thus exact. Similarly in Region IV, given that $\angle\mathbf{LCK}=\pi$ (*i.e.* perfectly behind the *lock*-particle), the expression reduces to $V_L(\mathbf{r},\mathbf{c})=V_L(z_{\overline{LK}}(\mathbf{r},\mathbf{c}))$ and is thus also exact.
- When $c\le R_L\cos(\angle\mathbf{RLC})$, then Region II disappears. Note that $\angle\mathbf{RLC}$ is independent of c.

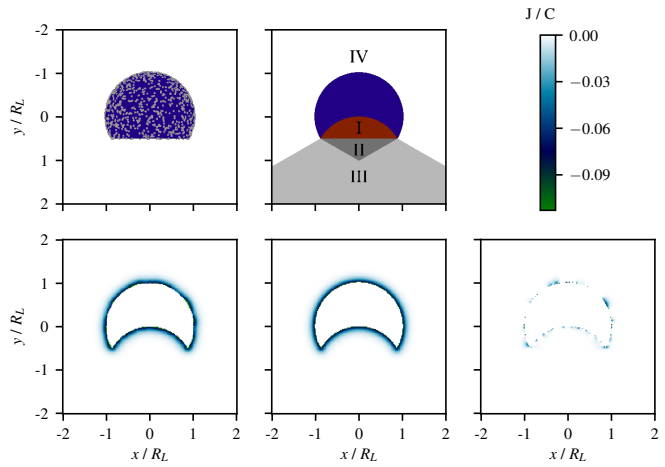

Fig. S3 Potential from (lower-left) 10000 randomly distributed particles on the surface of a *lock*-particle and (lower-middle) the approximate potential using Eq. S12. The far right panel shows the difference between the two models. The screening for both figures was $10^{-4}M$. The upper figures illustrates the respective models.

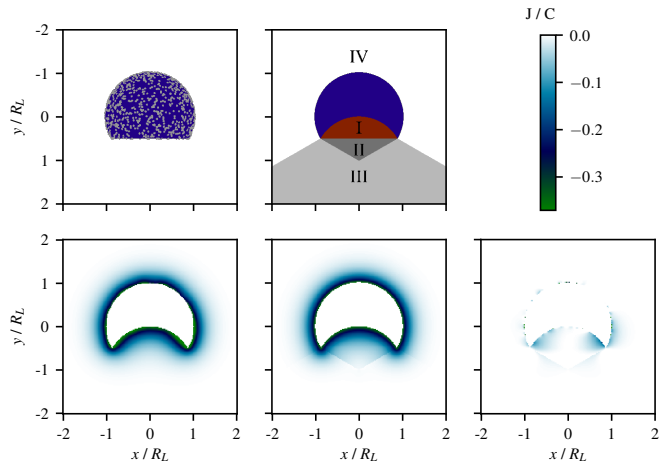

Fig. S4 Potential from (lower-left) 10000 randomly distributed particles on the surface of a *lock*-particle and (lower-middle) the approximate potential using Eq. S12. The far right panel shows the difference between the two models. The screening for both figures was $10^{-5}M$. The upper figures illustrates the respective models.

- When $c = 0$, then the cavity is either (assuming $R_C < R_L$) enclosed by the sphere $(\mathbf{L}, R_L)$, or (assuming $R_C \geq R_L$) enclosing the entire volume of the *lock*-particle.
- When $c + R_C < R_L$, the cavity is enclosed by the sphere $(\mathbf{L}, R_L)$ and thus by using a hard overlap potential no *key*-particle can penetrate into the cavity.

Simulation results

Results using $R_K = 0.8R_L$

In Fig. S6, we show configurations from simulations where higher order structures are formed for low degree of indentation and low number ratios, $N_L/N_K = \{1,2\}$. For $N_L/N_K = 1$, short dipolar chains coexist with larger aggregates. For $N_L/N_K = 2$, the two particles form aggregates with no clear ordering.

Results using $R_K = R_L$

In Fig. S7, the number of specific, unspecific and total bonds are presented for simulations using $R_K = R_L$. We observe that the specific bonds are predominant in most cases, but that the assembly becomes more unspecific at the lowest ionic strengths. The maximum number of specific bonds realized is larger than by using $R_K = 0.8R_L$. From an energetic point of view, the electrostatic contribution is maximized while matching the curvatures of the cavity and the *key*-particle, and here overcomes the entropic cost. In addition, as the *key*-particle is larger than by using $R_K = 0.8R_L$, more *lock*-particles can assemble at the surface of a *key*-particle and the total number of bonds is larger. With decreasing indentation, the assembly is shifted to lower ionic strength and the increase of the number of bonds become sharper. After this point the number of specific and total bonds is enhanced by shifting the indentation slightly outwards, while before this point the number of specific and total bonds is the largest for low c. For high N_L/N_K ratios the spherical *lock*-particle generally gives the highest yield of bonds, yet for smaller ratios the indentations does not have an hampering effect with regard to maximizing the total number of bonds. For large ionic strengths an indentation does even seem to promote more bonds as compared to no indentation.

Results using $R_K = 1.2R_L$

Typical simulation snapshots generated with $N_L/N_K = 1$ at different ionic strengths including the uncharged conditions ($\sim$ infinite screening) are shown in Fig. S8 (top) where the size of the *key*-particles was set to $R_K = 1.2R_L$, which is slightly larger than the *lock*-particles and their cavities. In Fig. S9, the number of specific, unspecific and total bonds are presented for simulations using $R_K = 1.2R_L$. All but the $N_L/N_K = 10$ ratio shows larger clusters consisting of more than one *key*-particle. We observe that the unspecific bonds are predominant in most cases, and only for $c = 1.2 - 1.4R_L$ is the number of specific bonds comparable to the number of unspecific ones. The maximum number of specific bonds is generally lower than by using $R_K = R_L$, akin the $R_K = 0.8R_L$ results. For large R_K, the entropic contribution is roughly independent of R_K, see Fig. 1 in main article, and thus it is primarily the energetics which differs between the $R_K = R_L$ and $R_K = 1.2R_L$ systems. Again, from an energetic point of view, the electrostatic contribution is maximized while matching the curvatures of the cavity and the *key*-particle, and thus it is not surprising that the $R_K = R_L$ results shows more specificity than by using $R_K = 1.2R_L$. However, as the *key*-particle is larger more *lock*-particles can assemble at the surface of the *key* and the total number of bonds is larger than by using a smaller R_K. The *key*-particles seem to maximize the total number of bonds which forces systems with small N_L/N_K ratios to aggregate their clusters which in turn leads to formation of higher order structures. However, for large number ratios this is not necessary since the valancy shell is already saturated. Interestingly, the maximal number of specific bonds is generally retrieved using $N_L/N_K = 4$

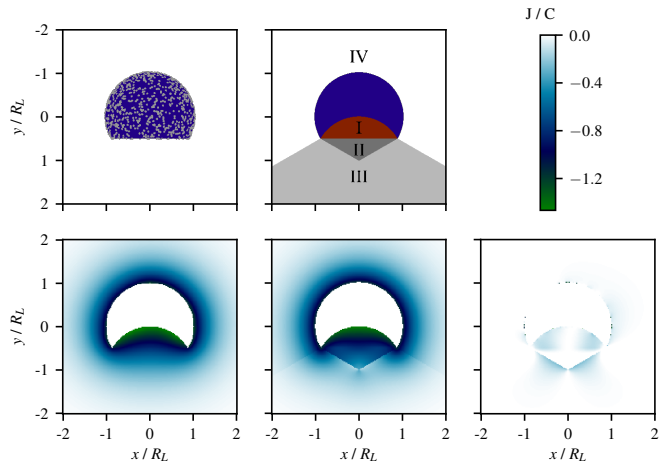

Fig. S5 Potential from (lower-left) 10000 randomly distributed particles on the surface of a *lock*-particle and (lower-middle) the approximate potential using Eq. S12. The far right panel shows the difference between the two models. The screening for both figures was $10^{-6}M$. The upper figures illustrates the respective models.

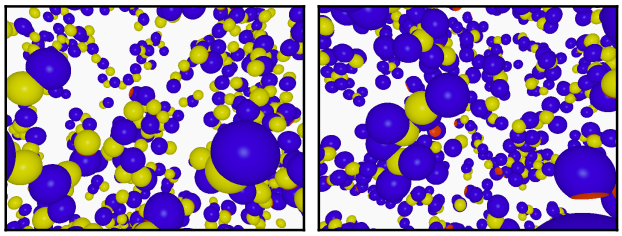

Fig. S6 Configurations from simulations using (left) $N_L/N_K = 1$ and (right) $N_L/N_K = 2$, $I = 10^{-5}$ M, $c = 1.6R_L$, and $R_K = 0.8R_L$.

and not by using $N_L/N_K = 10$. Thus by increasing N_L/N_K from four to ten the total number of bonds increase while the specific number of bonds decrease. This points toward many-body effects in the system, and that unbound *lock*-particles rather interact with unspecifically bound *lock*-particles rather than specifically bound ones. The number of specific bonds is enhanced by shifting the indentation slightly outwards, seemingly for any ionic strength.

Impact of cavity indentation

In Fig. S10, the number of bonds is presented for different R_K as a function of the degree of indentation. The number of specific bonds seems to have a maxima at $R_K = R_L$ independently of the degree of indentation. The peak of the *LK* curves seems to shift towards lower c as R_K is increased. Interestingly, the peak value of the total number of bonds is seemingly always higher by using an indentation than by not using one, independently of c and R_K. Another interesting feature is the local minima in unspecific bonds for $R_K = 1.2R_L$. The total number of bonds using $R_K = 1.2R_L$ is fairly constant (at least for high number ratios) and thus the shift in cavity does only shift the particles from back to front or vice versa.

Encapsulation

Four simulation snapshots obtained for two different surface charge-densities at $I = 10^{-5}$ M with $N_K/N_L = \{1,4\}$ are shown in Fig. S11. At $|\sigma| = 3.183 \cdot 10^{-4}$ e/nm^2, most of the *key*-particles were found to be freely dispersed. By charging up both types of particles by a factor $\sqrt{10}$, the entropic barrier for encasulation was overcome, which lead to the almost complete encapsulation of all *key*-particles by the "Pac-Man"-like *lock*-particles.

Impact of cavity radius

In Fig. S12 we present configurations from simulations where the radius of the cavity perfectly matches the radius of the *key*-particle, *i.e.* $R_C = R_K$, (left) and when it does not, *i.e.* $R_C < R_K$, (right). The total number of bonds per *key*-particle is roughly the same, ~ 9, however for a geometrically perfect match between the cavity and the *key*-particle the specific number of bonds is ~ 8 while the same number using $R_C < R_K$ is ~ 0. Here it is obvious that the impact of R_C is great, and that one basically can tune which types of bonds are included in the assembly.

References

1 J. Borovička, S. D. Stoyanov and V. N. Paunov, *Physical Review E*, 2015, **92**, 032730.

2 B. Beresford-Smith, D. Y. Chan and D. J. Mitchell, *Journal of colloid and interface science*, 1985, **105**, 216–234.

3 R. Kjellander and D. J. Mitchell, *The Journal of chemical physics*, 1994, **101**, 603–626.

4 M. Trulsson, J. Forsman, T. Åkesson and B. JoÌĹnsson, *Langmuir*, 2009, **25**, 6106–6112.

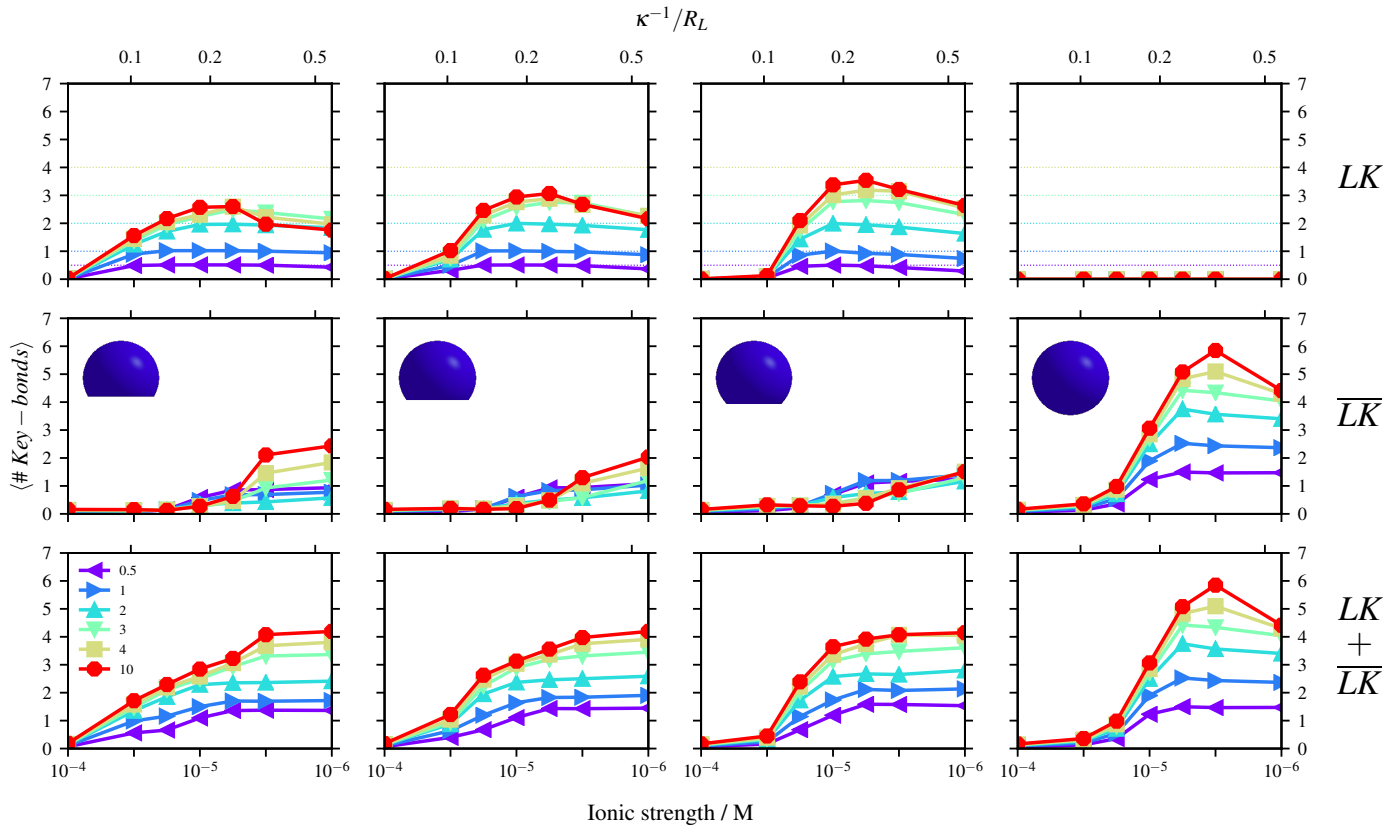

Fig. S7 Number of specific (top), unspecific (middle), and total (bottom) bonds per *key*-particle. The radius of the *key*-particle was $R_K = R_L$. The figures show results using: $c = 1.0R_L$ (far left), $c = 1.2R_L$ (left), $c = 1.4R_L$ (right), and $c = 2R_L$ (far right), for different ratios N_L/N_K according to the legend.

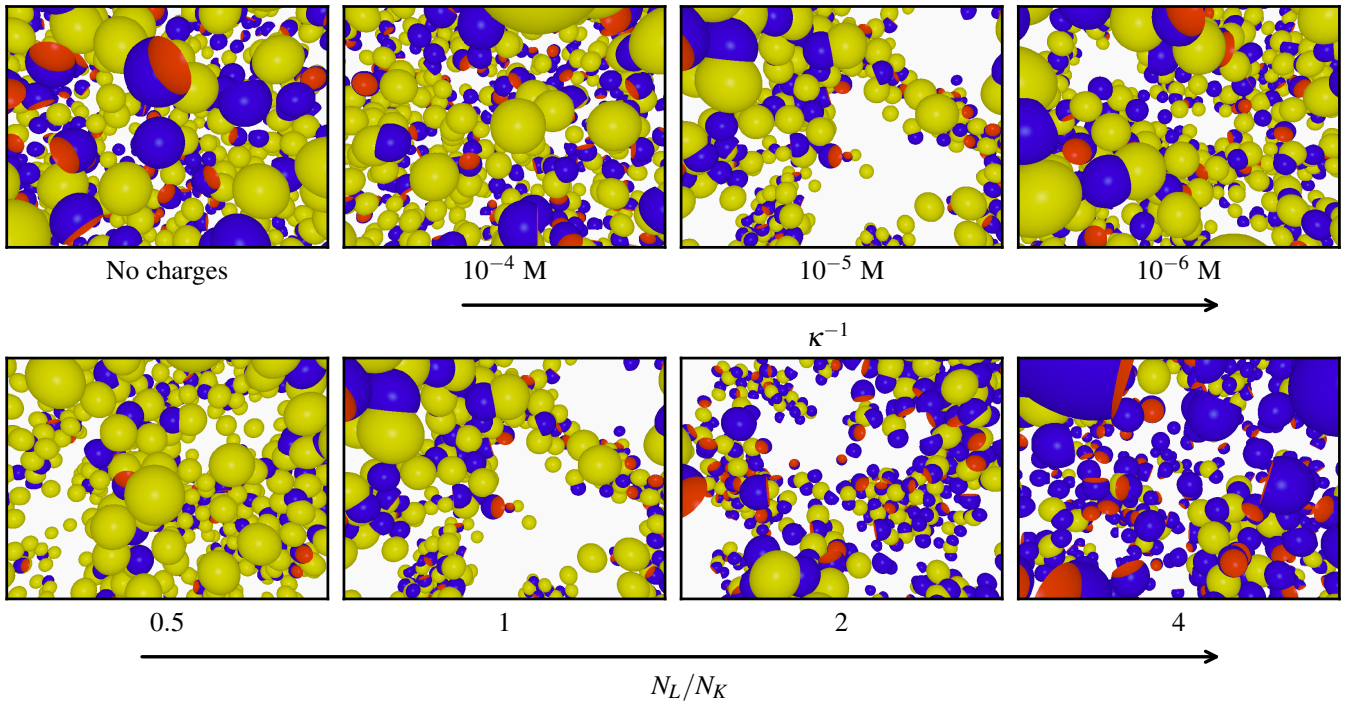

Fig. S8 (top) Configurations from simulations using $N_L/N_K = 1$ for different ionic screenings and (far left) no charges ($\sim$ infinite screening). (bottom) Configurations from simulations using $I = 10^{-5}$M for different ratios N_L/N_K. The *lock*-particles are described by $R_C = c = R_L$ and the *key*-particles by $R_K = 1.2R_L$.

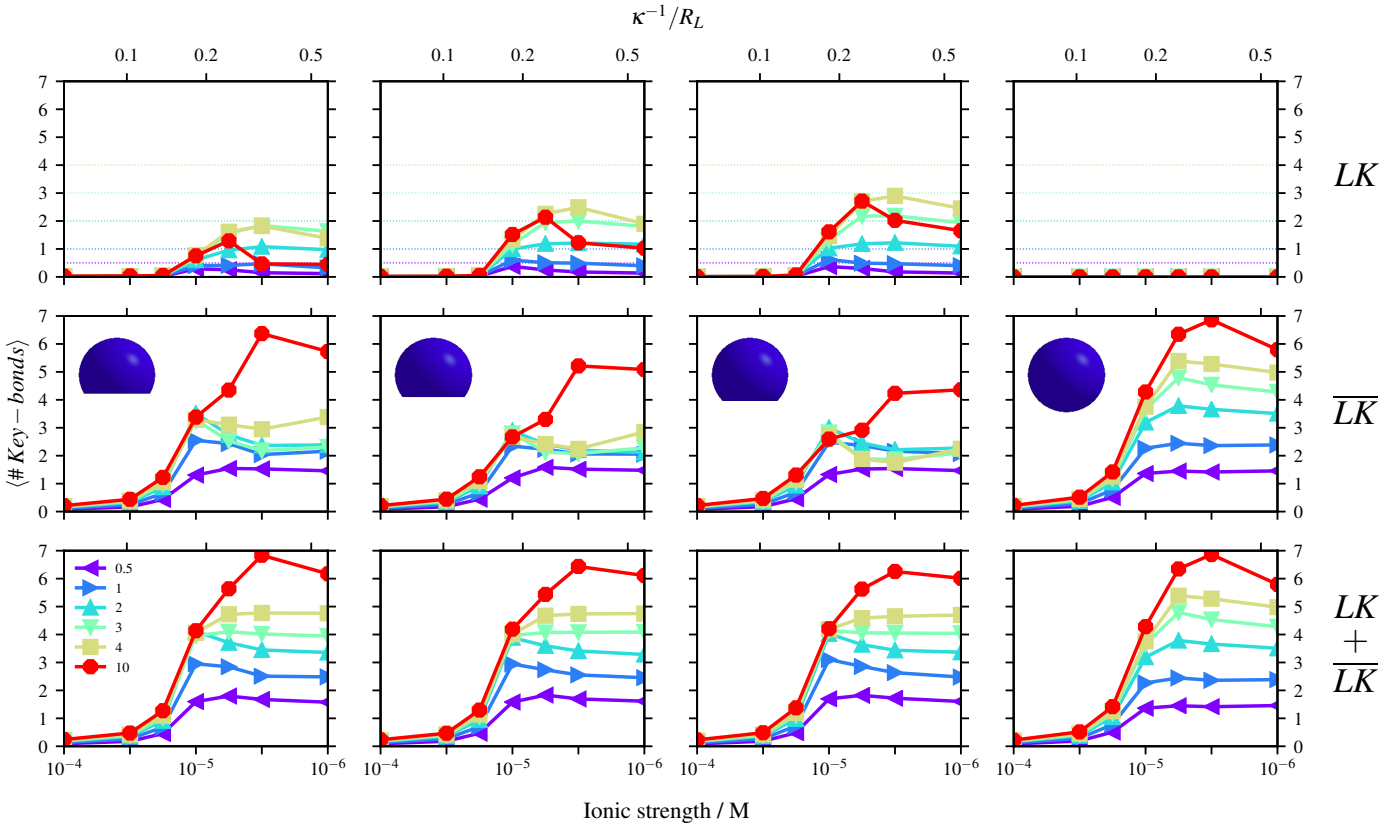

Fig. S9 Number of specific (top), unspecific (middle), and total (bottom) bonds per *key*-particle. The radius of the *key*-particle was $R_K = 1.2R_L$. The figures show results using: $c = 1.0R_L$ (far left), $c = 1.2R_L$ (left), $c = 1.4R_L$ (right), and $c = 2R_L$ (far right), for different ratios N_L/N_K according to the legend.

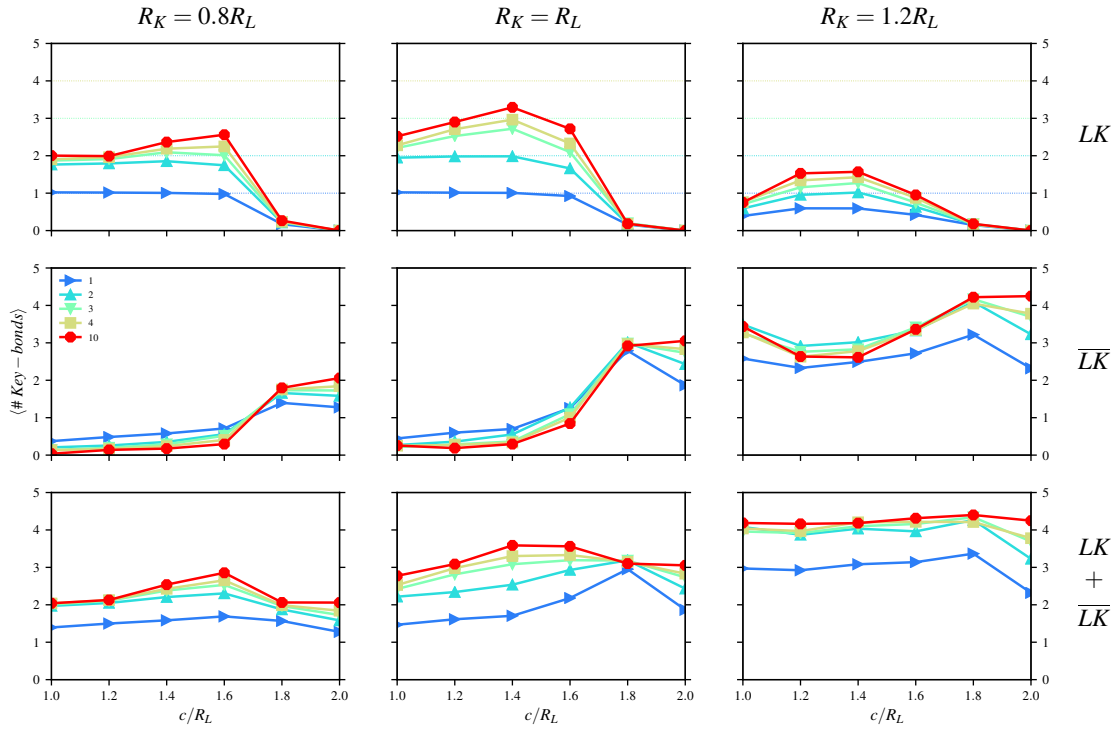

Fig. S10 Number of specific (top), unspecific (middle) and total (bottom) bonds per *key*-particle as a function of the degree of indentation. The radius of the *key*-particle is indicated above the columns. The figures show results using different ratios N_L/N_K according to the legend at ionic strength $I = 10^{-5}$ M.

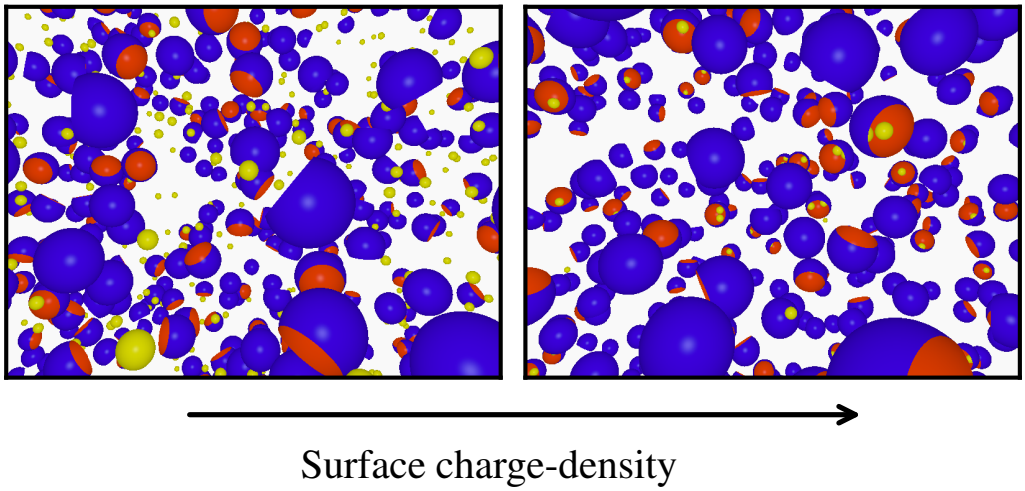

Fig. S11 Configurations from simulations using $N_K/N_L = 1$, ionic strength 10^{-5} M, $c = 0.1R_L$, $R_C = 0.95R_L$, and $R_K = 0.3R_L$. The left configurations are sampled by using the same surface charge-density as described in Sec. III, the right configurations used the same scaled with $\sqrt{10}$.

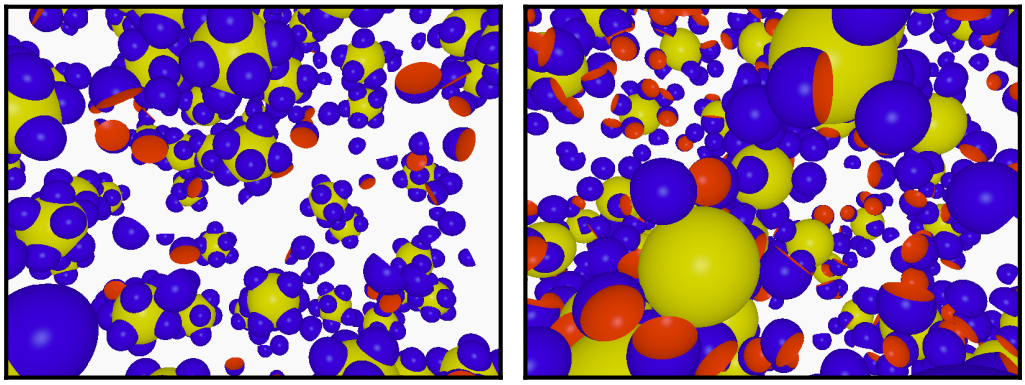

Fig. S12 Configurations from simulations using $N_L/N_K = 10$, ionic strength 10^{-5} M, and $R_K = 2.0R_L$. The left configuration is sampled by using $c = R_C = R_K$ (*i.e.* perfect geometric match between cavity and *key*-particle) and the right by using $c = R_C = R_L$.